

# Phase Separation and the Phase Diagram in Cuprates Superconductors

E. V. L. de Mello\* and D. H. N. Dias  
*Instituto de Física, Universidade Federal Fluminense,  
Niterói, RJ 24210-340, Brazil*

Otton Teixeira da Silveira Filho  
*Instituto de Computação, Universidade Federal Fluminense,  
Niterói, RJ 24210-340, Brazil*

(Dated: April 21, 2022)

We show that the main features of the cuprates superconductors phase diagram can be derived considering the disorder as a key property of these materials. Our basic point is that the high pseudogap line is an onset of phase separation which generates compounds made up of regions with distinct doping levels. We calculate how this continuous temperature dependent phase separation process occurs in high critical temperature superconductors (HTSC) using the Cahn-Hilliard approach, originally applied to study alloys. Since the level of phase separation varies for different cuprates, it is possible that different systems with average doping level  $p_m$  exhibit different degrees of charge and spin segregation. Calculations on inhomogeneous charge distributions in form of stripes in finite clusters performed by the Bogoliubov-deGennes superconducting approach yield good agreement to the pseudogap temperature  $T^*(p_m)$ , the onset of local pairing amplitudes with phase locked and concomitantly, how they develop at low temperatures into the superconducting phase at  $T_c(p_m)$  by percolation.

PACS numbers: 74.72.-h, 74.80.-g, 74.20.De, 02.70.Bf

## I. INTRODUCTION

After almost twenty years of research, the high critical temperature superconductors (HTSC) still remains as an unsolved problem[1, 2, 3]. All HTSC have a similar universal complex electronic phase diagram: the parent (undoped) compound is an antiferromagnetic Mott insulator, the superconducting phase has a dome shape at low doping and low temperature. The normal phase has a pseudogap in the underdoped region at low temperatures and a metallic phase at high temperatures in the overdoped region. Understanding the complexity of such normal phase is believed to be essential for solving the mechanism of HTSC[1].

Another intriguing fact is the question of the inhomogeneities in these materials; some families of compounds have a high inhomogeneous electronic structure which display either stripe[4], patchwork[5], checkerboard[6], or other forms[7]. On the other hand, depending on the type of experiment, there are some HTSC materials that appear to be more homogeneous or, at least do not display any gross inhomogeneity[8, 9]. It is possible that these distinct features are due to a phase separation transition that produces different degrees of local hole doping densities and consequently, different properties. We have already discussed this possibility in a previous paper[10] and we now perform more detailed calculations in con-

nections with several new experimental data.

Recent angle resolved photoemission (ARPES) experiments with improved energy and momentum resolution[11, 12, 13, 14] have distinguished two electronic components in  $\vec{k}$ -space associated with the  $La_{2-x}Sr_xCuO_4$  (LSCO) system: a metallic quasi particle spectral weight at the  $(\pi/2, \pi/2)$  nodal direction which increases with hole doping and an insulator like spectral weight at the end of the Brillouin zone straight segments in the  $(\pi, 0)$  and  $(0, \pi)$  antinodal regions which are almost incentive to the doping level. Comparison with the non superconducting  $La_{2-x-y}Nd_ySr_xCuO_4$  system[12], in which static stripes were first observed[4], demonstrated that the antinodal spectral weight behavior is compatible with a quasi one dimensional electronic structure where the hole rich stripes behaves as one dimensional metals and the hole poor stripes as insulators. These features demonstrated that in these compounds there are two aspects of the electronic structure[11, 12, 13, 14]. Moreover, the large shift of the ARPES spectra[11] at the Fermi energy, what is called the *leading edge shift* and it is interpreted as the superconducting gap is maximum at the antinodal region. This is an indication of the d-wave symmetry of the superconducting order parameter, the zero temperature superconducting gap  $\Delta_0$  vanishes in the nodal but it is maximum in the antinodal directions.

Another technique which has been refined and revealed new aspects of HTSC is scanning tunneling microscopy (STM). It is complementary to ARPES because it probes the differential conductance or the pairing amplitude  $\Delta$

---

\*evandro@if.uff.br

directly on the surface of the compound. New STM data with great resolution have also revealed strong inhomogeneities in the form of a patchwork of (nanoscale) local spatial variations in the density of states which is related to the local superconducting gap[5, 15, 16]. More recently it was possible to distinguish two distinct behavior: well defined coherent and ill-defined incoherent peaks depending on the exactly spectra location at a  $Bi_2Sr_2CaCu_2O_{8+\delta}$  (Bi2212) surface[17, 18, 19]. STM experiments have also detected a regular low energy checkerboard order in the electronic structure of the Bi2212 family above the superconducting critical temperature ( $T_c$ )[21] and at low temperature[20] and in the  $Na_xCa_{2-x}CuO_2Cl_2$ [6].

A third important set of experiments to describe the HTSC phase diagram is the tunneling current[22, 23, 24]. New techniques have recently shown the existence of two energy gaps which behaved differently under an applied magnetic field[25, 26, 27]. Tunneling experiments using superconductor insulator superconductor (SIS) with insulator layers with various size and resistivity have also shown distinct sets of energy scales and have also led to the idea that the richness of the phase diagram as function of doping may be due to charge inhomogeneities and charge cluster of different size in the Cu-O planes[28, 29].

The ARPES and STM experiments, are surface probes what may suggest that the inhomogeneities may be a surface effect, but charge disorders were also detected by bulk experiments, like the stripe phase in materials similar to LSCO[4, 30] and also local variations in the charge [31]. Another bulk sensitive experiment is nuclear magnetic and quadrupole resonance (NMR and NQR) which have provided ample evidence for spatial charge inhomogeneity in the  $CuO_2$  planes[32, 33, 34]. Similarly, Singer et al[33] measured a distribution of  $T_1$  over the Cu NQR spectrum in bulk LSCO which can be attributed to a distribution of holes  $p$  with a half width of  $\Delta p/p \approx 0.5$ . More recently, NMR results on  $La_{1.8-x}Eu_{0.2}SrCuO_4$  were interpreted as evidence for a spatially inhomogeneous charge distribution in a system where the spin fluctuations are suppressed[35]. This new result is a strong indication that the charge disorder may be due to a phase separation transition.

These unusual features of cuprates led to theoretical proposals that phase separation is essential to understand their physics[36, 37]. In fact, phase segregation has been observed on the  $La_2CuO_{4+\delta}$  by x-ray and transport measurements[38, 39]. They have measured a spinodal phase segregation into an oxygen-rich (or hole-rich) metallic phase and an oxygen-poor antiferromagnetic phase above  $T=220K$ . Below this temperature the mobility of the interstitial oxygen becomes too low for a further segregation.  $La_2CuO_{4+\delta}$  is the only system where ion diffusion has been firmly established, although there are evidence of ion diffusion at room temperature in micro crystals of the Bi2212 superconductors at a very slow rate[40].

On the other hand, recent NMR studies on

$YBa_2Cu_3O_{6+y}$  (YBCO) have demonstrated a complete absence of static phase separation or at least an absence of gross inhomogeneities[8, 9]. Contrary to what was measured in Bi2212 and in LSCO, the maximum hole doping variation  $\Delta p$  found in YBCO is very small[8]. Loram et al[9] analyzed also the specific heat of YBCO and Bi2212 and concluded that there are evidences for an uniform doping density in these materials. Surface measurements are difficult to be performed in YBCO and therefore they are not as conclusive as in Bi2212 or LSCO[8, 11].

In this paper we develop the idea of two distinct[41] pseudogaps in which the lower one is associated with the onset of superconductivity[42]. We then take the upper pseudogap line as a line of phase separation transition, and introduce a model to make quantitative predictions through the Cahn-Hilliard (CH) approach[10, 43, 44] in section II. In this way, gross and weak disordered systems differ only by the degree of mobility or diffusion of the particles and different systems can belong to the same universality class. In section III we use the Bogoliubov-deGennes (BdG) local method to the superconducting problem to calculate the local pairing amplitude in mesoscopic clusters with random, stripes, checkerboard, Gaussian and other forms of inhomogeneities in the charge density. The results on stripe-like formations applied to the LSCO system reveal a pseudogap phase characterized by the building up of superconducting islands or puddles with, as in BCS theory, the phase locked. Consequently the superconducting phase is reached at low temperatures by the percolation of these islands[45, 46, 47]. The details of these calculations are discussed in section II and III with their consequences to HTSC in section IV.

## II. THE CH APPROACH

Our main assumption is that the high pseudogap line, which we call  $T_{ps}(p_m)$ , falls to zero near  $p \approx 0.20$ , and is independent of the superconducting phase[3, 48], is the onset of the phase separation. Timusk and Sttat called this line a crossover boundary[2] and it is distinct of the lower pseudogap[42]. Thus a given system start to phase separate at  $T_{ps}(p_m)$  and this process increases continuously as the temperature goes down.

Thus the phase separation problem in HTSC is a dynamical and depends strongly on the initial conditions, on the temperature and how the system is quenched below the phase separation line, the mobility of hole and ions, and so on. However, the information on most of these procedures are not available and one has to work out the phase separation process backwards, to wit, use parameters which yield the final configurations of stripe, checkerboard, or other patterns. An appropriate framework to study such process mathematically is by the CH theory[43], which we have already applied to the cuprates[10].

The CH approach to phase separation was conceived to

describe the continuous transition of binary alloys, but, in principle, can be applied to any system that undergoes this type of continuous transition[43]. As we can infer from the stripe phases, in a compound with an average of  $p_m = 1/8$  hole per copper atom, the antiferromagnetic insulating phase has stripes of nearly zero holes per copper atom and metallic ones with larger values of local charge density. As we discuss below, this behavior can be well described by the CH theory.

Starting with small fluctuations of the local charge density, the CH non-linear differential equation which describes the phase separation at a temperature  $T$  below the phase separation transition at  $T_{ps}$  can be written as[10, 43]:

$$\frac{\partial u}{\partial t} = -M\nabla^2(\varepsilon^2\nabla^2u + A^2(T)u - B^2u^3), \quad (1)$$

where  $u$  is the order parameter associated with the local variation  $p(\vec{x})$  in the average number of holes per copper atom  $p_m$  at a given point  $\vec{x}$ , defined as  $u(\vec{x}) \equiv p(\vec{x}) - p_m$  and we expected  $u(\vec{x}) \approx 0$  above and near the  $T_{ps}$ .  $\varepsilon$ , and  $B$  are fixed parameter, the parameter  $A(T)$  depends on the temperature  $T$  and  $B$  and the ratio  $\pm A(T)/B$  yields the two equilibrium densities.  $M$  is the mobility of the particles and dictates the time scale of the phase separation process. Compounds with larger values of  $M$  phase separate easier than those with smaller values, and, therefore, it will differentiate among the different HTSC families. As the temperature goes down below  $T_{ps}(p_m)$ , the two equilibrium order parameter (or densities) spread apart from one another and the energy barrier between the two equilibrium phases  $E_g(T, p_m)$  also increases.  $E_g = A^4(T)/B$  which is proportional to  $(T_{ps} - T)^2$ .  $E_g$  can be identified with the upper pseudogap signal[10] which is detected by several different experiments[3, 42]. A discussion on the details of the convergence criteria, boundary conditions and dependence on the initial parameters in one, two or three dimensions, can be found in our previous work[44].

In Figs.(1) and (2) we display the mapping of the order parameter for a system with  $p_m = 1/8$  and with a maximum  $\Delta p = 1/8$ . Both figures have a small initial density fluctuation of  $\Delta p = 0.02$  but Fig.(1) has more random initial conditions than the more symmetric case of Fig.(2). We notice that, for larger times they are almost indistinguishable but for short times they are very different. It is interesting that, despite the large time evolution, the system keeps very symmetric patterns. In Fig.(2a) we can see a mixture of checkerboard and stripe formations which tends to evolve into a pure stripe phase (Fig.(2b)). As the phase separation process continues, the systems tends to a complete phase separation and the early symmetric patterns are lost. This degree of charge phase separation can be reached very fast if the holes have a large mobility  $M$ . This finding enable us to speculate that the differences measured among the HTSC families are due to different values of  $M$ . By the same token, the differences found in compounds of a given family

can be attributed to differences in the quenched process, that is, the rate of cooling below  $T_{ps}(p)$ .

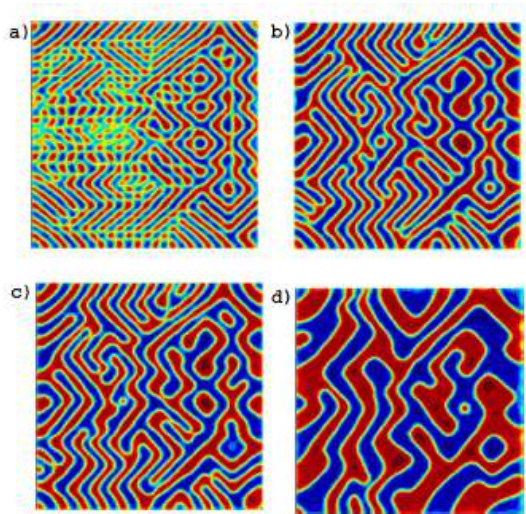


FIG. 1: (color online) The mapping of the density order parameter during the process of phase separation. The start order parameter is small random variations around  $u = 0$ . The order of the figures is a)  $t=400$  time steps, b)  $t=800$ , c)  $t=1000$  and d)  $t=4000$ .

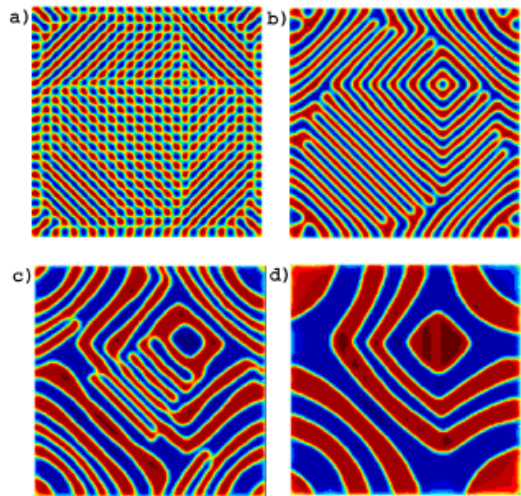


FIG. 2: (color online) The same time evolution of Fig.1 but with a more symmetric initial condition around  $u = 0$ . The order of the figures is a)  $t=400$  time steps, b)  $t=1000$ , c)  $t=4000$  and d)  $t=20000$ . For shorter times, the phase separation process develops symmetry patterns which are lost for larger times.

Another possible way to follow the whole phase separation process is to analyze the charge histogram evolution with time. Thus, in Fig.(3) we show the phase separation progress in terms of the histograms of the order parameter. One can see the tendency, as the time flows, to form

a density pattern of a bimodal distribution around the two equilibria conditions  $p(i)_\pm = \pm A/B$ . Thus, systems with a high mobility will probably reach a state where there are two type of regions with high and low densities. This is similar to the stripe phase in the LSCO system.

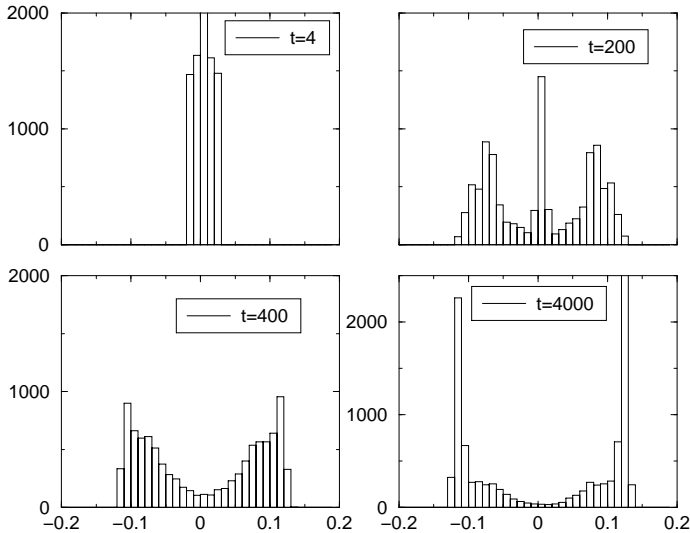


FIG. 3: The histogram time evolution of the density order parameter of Fig.1 with a symmetric initial condition around  $u = 0$ .

Therefore, taking the large pseudogap[3, 10, 48] as the phase separation temperature  $T_{ps}$ , it is possible to infer that the different HTSC unfold in different patterns as described by Figs. 1 and 2. As a consequence, since underdoped compounds have a very high  $T_{ps}$ , they phase separate into a bimodal distribution faster than the optimally and overdoped compounds. The NQR results of Singer et al[33] suggest a bimodal distribution of charge in the LSCO system.

Thus, in order to calculate the local critical temperature for such an inhomogeneous system, we need to use the Bogoliubov-deGennes theory. This will be outlined in the next section.

### III. THE LOCAL SUPERCONDUCTING CALCULATIONS

Here we discuss the main points of a local superconducting calculation to deal with the effect of the charge disorder which follows directly from the CH patterns described above. The general way to perform this, in a system without spatial invariance, is through the BdG mean-field theory which has been largely used in the HTSC problem[49, 50, 51, 52]. The important and novel point introduced here is that we take the initial charge distribution derived from the CH results. The procedure starts with the extend Hubbard Hamiltonian

$$H = - \sum_{\langle\langle ij \rangle\rangle\sigma} t_{ij} c_{i\sigma}^\dagger c_{j\sigma} + \sum_{i\sigma} (\mu_i) n_{i\sigma} + U \sum_i n_{i\uparrow} n_{i\downarrow} + \frac{V}{2} \sum_{\langle ij \rangle\sigma\sigma'} n_{i\sigma} n_{j\sigma'} \quad (2)$$

where  $c_{i\sigma}^\dagger$  ( $c_{i\sigma}$ ) is the usual fermionic creation (annihilation) operators at site  $\mathbf{x}_i$ , spin  $\sigma \{\uparrow\downarrow\}$ , and  $n_{i\sigma} = c_{i\sigma}^\dagger c_{i\sigma}$ .  $t_{ij}$  is the hopping between site  $i$  and  $j$ . Here we have implemented in our calculations hopping values up to 5<sup>th</sup> neighbors derived from the ARPES data for YBCO[53]. In their notation, the hopping parameters are:  $t \equiv t_1=0.225\text{eV}$ ,  $t_2/t_1=-0.70$ ,  $t_3/t_1=0.25$ ,  $t_4/t_1=0.08$ ,  $t_5/t_1=-0.08$ .  $U = 1.1t$  is the on-site and  $V = -0.6t$  is the nearest neighbor phenomenological interactions.  $\mu_i$  is the local chemical potential. All the calculations presented here use the same set of parameters, and clusters with periodic boundary conditions.

$$\begin{pmatrix} K & \Delta \\ \Delta^* & -K^* \end{pmatrix} \begin{pmatrix} u_n(\mathbf{x}_i) \\ v_n(\mathbf{x}_i) \end{pmatrix} = E_n \begin{pmatrix} u_n(\mathbf{x}_i) \\ v_n(\mathbf{x}_i) \end{pmatrix} \quad (3)$$

These BdG equations are solved self-consistently together with the pairing amplitude[49]

$$\Delta_U(\mathbf{x}_i) = -U \sum_n u_n(\mathbf{x}_i) v_n^*(\mathbf{x}_i) \tanh \frac{E_n}{2k_B T}, \quad (4)$$

$$\Delta_\delta(\mathbf{x}_i) = -\frac{V}{2} \sum_n [u_n(\mathbf{x}_i) v_n^*(\mathbf{x}_i + \delta) + v_n^*(\mathbf{x}_i) u_n(\mathbf{x}_i + \delta)] \tanh \frac{E_n}{2k_B T}, \quad (5)$$

and the hole density is given by

$$p(\mathbf{x}_i) = 1 - 2 \sum_n [|u_n(\mathbf{x}_i)|^2 f_n + |v_n(\mathbf{x}_i)|^2 (1 - f_n)], \quad (6)$$

where  $f_n$  is the Fermi function.

We have performed self consistent calculations with Eqs.(5) and (6) on clusters up to  $24 \times 24$  sites with homogeneous and inhomogeneous local doping. The major difference from previous BdG calculations is that instead of an impurity potential[50, 51] to account for the charge disorder, we have fixed the initial local charge densities throughout the calculations in order to take into account the results of the CH approach and also in agreement with the data on stripe formation[4, 30]. This novel procedure is necessary to study the formation of the superconducting regions on the local density patterns which results from the phase separation process as shown, for instance, in Figs.1 and 2. In the next section, we perform the superconducting calculations with d-wave symmetry for clusters with disordered local charge.

#### IV. RESULTS

We start with BdG calculations on clusters of uniform density ranging from zero to  $p_m = 0.3$  with the hopping parameters which make the values of  $T_c(p_m)$  vanish near these limits as listed below Eq.2. Then we perform calculations with inhomogeneous clusters and concentrate on the stripe geometry which occur in LSCO[4]. We connect the stripe phase with the above CH results through a scheme displayed in Fig.(4) where the value of  $X$  is related with the degree of the phase separation. Due to the large values of  $T_{ps}(p_m)$  at the strong underdoped regime, the level of phase separation is maximum at low temperatures, and  $X = 0$  for doping values of  $p_m \leq 0.05$ . For  $0.12 \leq p_m \leq 0.19$  the value of  $X$  may build up to 0.05. Notice that when  $X=0$ , the charge distribution is a bimodal and the system is divided into two distinct regions; insulator and metallic. In this case the metallic regions are in the limit of percolation[54], but for  $X=0.04$  or bigger, despite of the insulator regions present, the metallic character dominates over the entire system. This scheme is an approximate way to deal with the phase separation which leads to the stripe charge configuration of real systems.

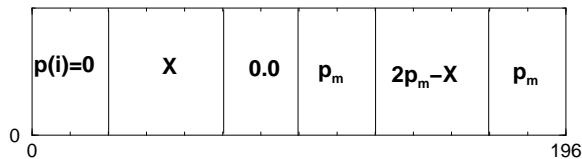


FIG. 4: The low temperature stripe profile of a  $14 \times 14$  cluster with 196 sites used to model a compound of average doping level of  $p_m$ . The BdG superconducting calculations are made on these clusters and  $0 \leq X \leq 0.06$  measure deviations from a bimodal charge distribution.

Thus, the goal is to study the *local* pairing gap at a site  $\mathbf{x}_i$  or simply "i" as function of temperature  $\Delta(i, T)$  on clusters with charge stripes. Following the values of  $\Delta(i, T)$  it is possible to draw many interesting consequences to the phase diagram. To explain our approach, we will firstly analyze the results for a cluster with  $p_m = 0.16$  in a  $14 \times 14$  cluster as shown in Fig.(5). At high temperatures but below  $T_{ps}(p_m = 0.16) \approx 400\text{K}$ [3], the system is a disordered metal going through a continuous phase separation as the temperature is decreased. At low temperatures ( $\leq 200\text{K}$ ) this compound may be composed of six stripes with local charge density  $p(i)$  given by  $0.0 - 0.05 - 0.0 - 0.16 - (0.32 - 0.05) - 0.16$ . The low density regions are at the left and the high density are at the right of the cluster and one follows the other by periodic boundary conditions. These two markedly different regions were clearly detected by several ARPES measurements[11, 12, 13, 14]. At high temperatures there is no superconducting regions in the sample, but at  $T^* = 65\text{K}$ , as we can see in Fig.(5), some local superconducting gap arises forming superconducting islands at

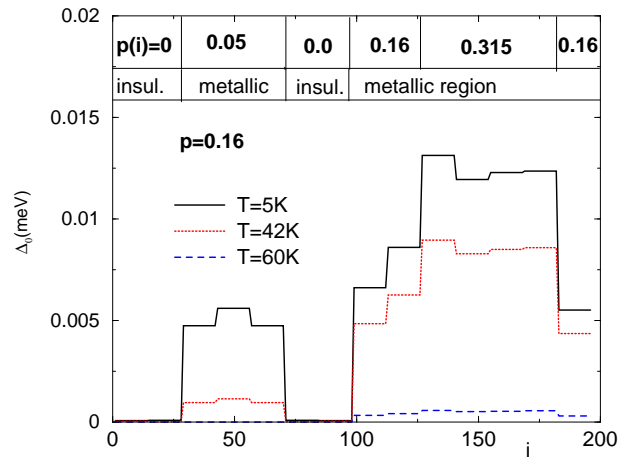


FIG. 5: (color online) The temperature evolution of the local pairing gap amplitude  $\Delta(i, T)$  (in units of eV) for systems with stripe disorder and average doping level of  $p_m = 0.16$  with  $T^* \approx 65\text{K}$  and  $T_c \approx 42\text{K}$ .

the most dense or metallic regions. Thus this temperature is the onset of pair formation or the beginning of the pseudogap phase but these superconducting regions are isolated from one another in the disordered metallic matrix[45, 46, 47]. Upon cooling down, the superconducting regions become more robust and new ones are built up at the metallic and also where there is a hole fluctuation (at  $X$  in Fig.(4)) at the lightly doped regions. The induced pairing amplitude at the insulator regions is an unexpected phenomena and it is remarkable that it is the origin of the superconducting phase through the percolation of the local superconducting order parameter at different locations with their phase locked. As seen in Fig.(5), around 42K the pairing amplitudes develop also at  $X = p(i) = 0.05$  but for the  $p_m = 0.06$  sample, they develop even at  $X = p(i) = 0.001$  (see Fig.(6)) and thus, the superconducting regions cover more than 50% of the  $\text{CuO}_2$  plane. Consequently they percolate[54] and the whole system is able to hold a current without dissipation, that is,  $T_c(p_m = 0.16) = 42\text{K}$  is the superconducting critical temperature for this compound.

Notice that the assumption that the pairing amplitudes have a rigid phase, as in a BCS superconductor, has also experimental support[55], although it is against the phase disordered scenario which lately has gained increased theoretical interest[7, 56].

We now apply this analysis to a series of compounds in order to show how the main features of the whole LSCO phase diagram can be derived. Our results are shown in Fig.(6) for mostly underdoped samples and in Fig.(7) for larger average doping values. For very lightly doped compounds like  $p_m = 0.03$ , due to the high values of  $T_{ps}(p_m)$ , there are stripes of only  $p(i) = 0.0$  and  $p(i) = 0.06$  separated by a small boundary with  $p(i) = 0.03$ . We label a region as metallic if it has a density of  $p(i) \geq 0.05$ , since the doped regions with  $p(i) = 0.06$  occupy less than half system, what is lower than the two dimen-



sional percolation limit of 50-60%[54], this compound is not a metal, although it has a metallic behavior at high temperatures[57]. Such behavior can be explained as due to the holes which can tunnel over the dense  $p(i) = 0.06$  regions. This tunneling can also be the origin of the zero temperature pseudo gap (ZTPG) detected by STM[18, 19, 20]. For these underdoped compounds, the pairing amplitude develops strictly in these metallic or heavy doped regions (see top panel of Fig.(7)), and the superconducting islands occupy less than 50% of the available area, what is below the percolation limit.

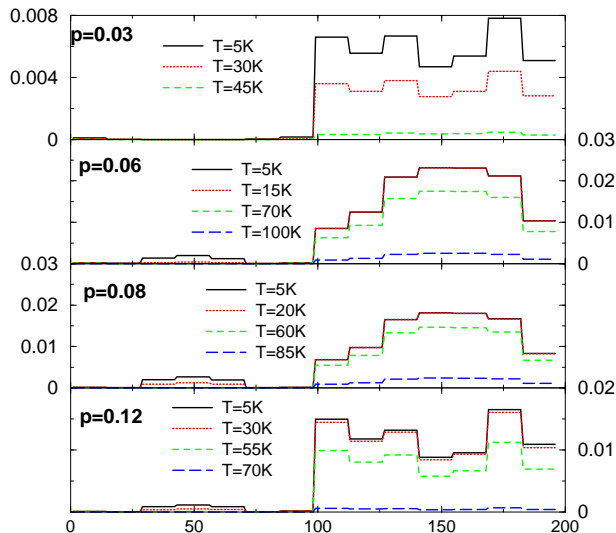


FIG. 6: (color online) The temperature evolution of the local pairing amplitude  $\Delta(i, T)$  (in units of eV) for systems with stripe charges with average doping level ranging from  $p_m = 0.03$  to  $p_m = 0.12$ . The onset temperature ( $T_c$ ) of percolation is shown in every panel

For a compound with  $p_m = 0.06$ ,  $T_{ps}$  is still very high, the density profile is characterized by a very small charge fluctuations around a bimodal distribution given by  $X = 0.001$ . The stripe regions have densities given by  $p(i) = 0.0 - 0.001 - 0.0 - 0.06 - 0.119 - 0.06$ . This system can be considered in the metallic limit which is 50% of the sites with  $p(i) \geq 0.04$ . We see that the onset of superconducting islands is at  $T^* = 100\text{K}$  and the percolation threshold occurs at  $T_c = 15\text{K}$ , specially due to the already mentioned unexpected pairing amplitudes induced at the low density sites with  $p(i) = 0.001$  (see Fig.(6)). Thus for temperatures between  $T = 15\text{K}$  and  $T = 100\text{K}$  the system is a poor metal with insulator, metallic and superconducting regions. The presence of these superconducting islands in many compounds are verified by several different experiments. Perhaps the most clear demonstration of these static superconducting regions is through the tunneling data[22, 29]. More recently, measurements of the Nernst effect[58] demonstrated also the presence of the local superconducting regions above  $T_c(p_m)$  although it was interpreted as due to superconducting fluctuations instead of the static cluster

considered here. For compounds with an average doping larger than  $p_m = 0.06$ , we notice that the onset of superconductivity  $T^*$  decreases almost steadily, while the onset of percolation  $T_c$  goes through a maximum at the optimum doping  $p_m = 0.16$ . The reason for this behavior in our calculation is the deviations from the bimodal distribution given by the increase of the phase separation parameter  $X$ .

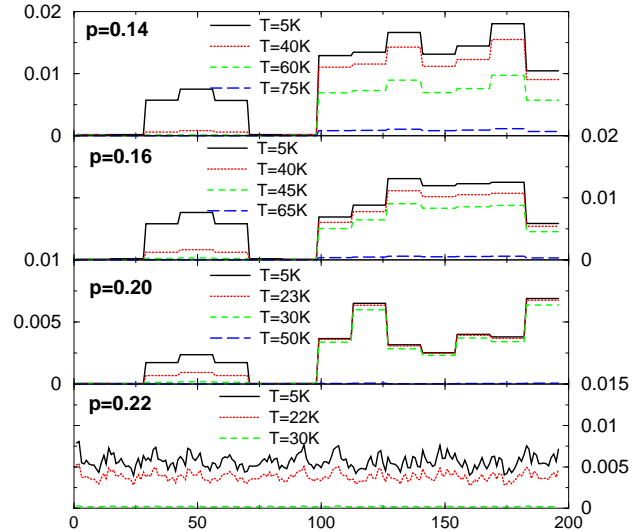


FIG. 7: (color online) The temperature evolution of the local pairing gap amplitude  $\Delta(i, T)$  (in units of eV) for systems with stripe disorder with average doping level ranging from  $p_m = 0.14$  to  $p_m = 0.22$ . Notice that the  $p_m = 0.22$  compound does not undergoes a phase separation transition and its density fluctuates around  $p_m = 0.22$ .

In the Fig.(7) we can see that the phase separation process and the local superconducting calculations follow a similar pattern up to  $p_m = 0.20$ . Following current trends[3, 42, 48], the phase separation ends at  $p_m \approx 0.20$  and, for heavier doped compounds, the charge disorder is very weak like a small fluctuation around the average value  $p_m$ , similar to the charge distribution shown in Fig.(3a). This is the same kind of charge fluctuation which occurs above the phase separation transition temperature  $T_{ps}$ . Consequently, the compound with  $p_m = 0.22$  differs greatly from the others compounds shown in Fig.(7), and it has only local densities  $p(i) \approx 0.22$  which is in the metallic range. The pairing gaps  $\Delta(i, T)$  are built in the whole system at  $T = 30\text{K}$  and not in islands or droplets. If we adhere to the assumption that the  $T^*$  is the onset of superconducting correlations, we see that, for these  $p_m \geq 0.20$  overdoped samples  $T^*$  merge into  $T_c$ . The other important consequence is that the normal phase is much more homogeneous, without insulating and superconducting regions, than the  $p_m \leq 0.20$  compounds. This is seen experimentally through the Fermi liquid behavior of many measurements carried in the heavy overdoped regime[2, 7].

In Fig.(8) we used the calculated local  $\Delta(i, T)$  on each

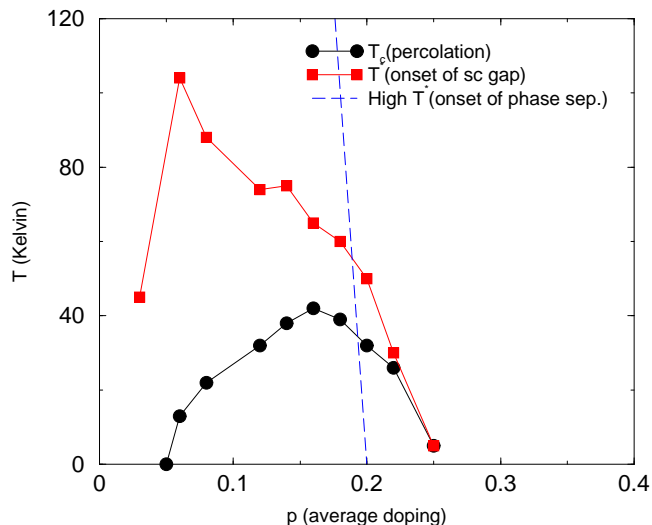


FIG. 8: (color online) The onset of superconducting islands temperature  $T^*(p_m)$  and the percolation temperature  $T_c(p_m)$  taken from Figs.(7) and (6). It is also shown the phase separation (dashed) line or upper pseudogap[3, 48].

compound to derive the LSCO phase diagram, to wit, the onset of superconducting temperature  $T^*(p_m)$  (squares) and the percolation temperature  $T_c(p_m)$ (circles) as function of  $p_m$ , as derived from Figs.(7) and (6). The values of  $T^*(p_m)$  are in good agreement with the measurements attributed to the lower pseudogap which is usually related with the onset of a superconducting property[2, 3, 42] as, for instance, the tunneling results[22, 29] and the Nernst effect[58]. The values of  $T_c(p_m)$  is also in good quantitative agreement with the experimental superconducting phase boundary[2, 3, 58].

We have also taken the larger superconducting gaps at low temperatures for each compound from Figs.(6) and (7) and plotted in Fig.(9). The calculated maximum gap for each compound at low temperature ( $\Delta_0(p_m)$ ) is in reasonable agreement with the ARPES zero temperature leading edge shift or the magnitude of the superconducting gap[14]. In this figure, just to show the effect of the disorder in our calculations, we have shown the values of  $\Delta_0(p_m)$  for homogeneous compounds. We see that the disorder increases the average zero temperature gap dramatically at low doping and in a weaker way, in the far overdoped regions. The discrepancies around optimally doped samples between the experimental values and our calculations are likely to be due to our approximate stripe configurations on small clusters.

It is important to notice that this stripe scheme is able to capture the very curious dual behavior of the electronic structure in LSCO systems[12]. At the lightly doped regime, due to the high values of the phase separation energy barrier  $E_g(T, p_m)$ , the charges move preferably along the high densities stripes, and the Cooper pairs are formed along them, as demonstrated in Figs.(6) and (7) by the calculated  $\Delta(i, T = 0K)$ . Consequently, with

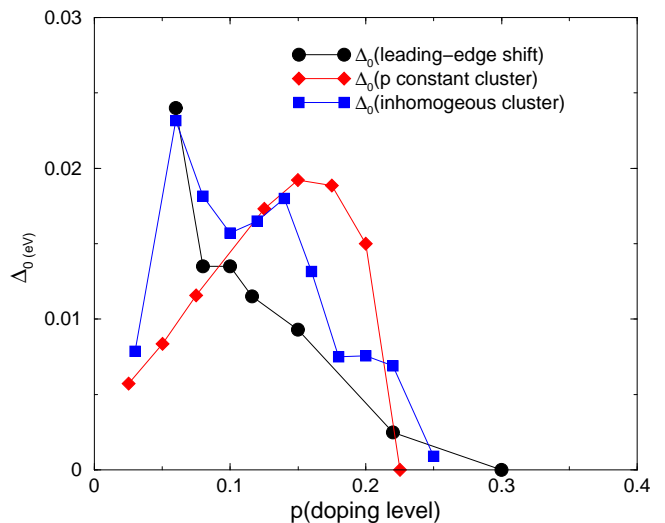


FIG. 9: The zero temperature superconductor gap as function of the doping level. The diamond points are for a cluster with uniform density. The square are for an inhomogeneous cluster according the CH results. The circles are the experimental leading edge gap from Ref.([14]).

a k-space probe, the superconducting gaps for lightly doped samples are measured mainly in the  $(\pi, 0)$  and  $(0, \pi)$  antinodal regions and the spectral weight segments are entirely near these antinodal regions. This behavior is expected for 1D stripes[12] and the measured values of the zero temperature leading edge as function of  $p_m$  can be qualitatively reproduced by the  $\Delta_0(p_m)$ , as shown in Fig.(9).

Since by assumption  $E_g(T, p_m)$  is closely related with the high pseudogap and, therefore decreases rapidly with  $p_m$ , it is easier to the holes in compounds near optimally doped than underdoped ones to tunnel over among the high and low doping stripes, yielding a 2D character to these systems. Thus as  $p_m$  increases, the samples tend to change continuously from 1D to a 2D metallic behavior and this is detected by the increase of the spectral weight near the Fermi surface along the  $[1,1]$  nodal direction[12]. Another evidence of the charge tunneling between different stripes is the presence of the incoherent ZTPG measured on the surface of Bi2212 compounds[18, 19] which should scaled with the energy barrier  $E_g(p_m, T)$ . The ZTPG are more frequently than the superconducting gap in the underdoped region and disappear near  $p_m = 0.19$ [18, 19, 20]. Evidence of these two types of gaps in HTSC compounds came also from tunneling experiments carried with different resistances[28, 29].

## V. CONCLUSIONS

We have worked out a complete scenario to HTSC and provided an interpretation to the upper and lower pseu-

dogap line and also to the superconducting phase. Taking the upper pseudogap as the phase separation temperature, we have calculated the local pairing amplitudes  $\Delta(i, T)$  which, as in BCS, is assumed to have their phase locked and the superconducting phase is reached by percolation at  $T_c(p_m)$ . In this way, we derived the phase diagram of the onset of  $\Delta(i, T)$ , that is  $T^*(p_m)$  and  $T_c(p_m)$  for a HTSC family. Although the process of phase separation varies continuously with the temperature and depends on the sample preparation, for simplicity, we use in our calculations only the low temperature static configuration. Despite this simplification, the method is quite general, and to demonstrate it, we reproduced results in good agreement with the LSCO series.

The many values of  $\Delta(i, T)$  in a single compound agrees with the several recent very fine STM maps on Bi2212 surfaces. The calculations with the CH stripe configuration have also provided novel interpretation to important aspects involved in the electronic structure of this type of disorder: the inhomogeneous electronic nature of underdoped LSCO cuprates measured by the straight (1D) segments near the anti nodal regions and the spectral weight near the nodal regions where the Fermi surface develops. The presence of the ZTPG peaks

in several Bi2212 compounds, as measured by high resolution STM data, may be due to the energy barrier between the low and high density regions in a given sample and therefore, in this view, is connected to the phase separation and not with the superconductivity. Our results indicate that the normal phase of cuprates is a disordered metal for  $p_m \leq 0.2$  composed by the coexistence of insulator and metallic regions below the phase separation temperature  $T_{ps}$ . These regions are composed of non constant hole density regions which yields a variety of local  $T_c(p(i))$  at low temperatures. This inhomogeneity is the source of scattering between these non-uniform regions, Andreev reflection, etc, what is the cause of many nonconventional transport properties[2, 7]. The study of these normal phase properties will be matter of future publication.

Thus, in short, with the combination of the CH phase separation model with the BdG superconducting theory, we have shown that the phase diagram and some non-conventional properties of HTSC receive a coherent interpretation based on a temperature dependent static phase separation.

This work has been partially supported by CAPES, CNPq and CNPq-Faperj Pronex E-26/171.168/2003.

- 
- [1] See discussion in Nature Physics **vol.2**, no. 3, (March of 2006).
- [2] T. Timusk and B. Statt. Rep. Prog. Phys. **62**, 61 (1999).
- [3] J. L. Tallon and J. W. Loram, Physica C **349**, 53 (2001).
- [4] J.M.Tranquada, B.J. Sternlieb, J.D. Axe, Y. Nakamura, and S. Uchida, Nature (London),**375**, 561 (1995).
- [5] S. H. Pan et al., Nature, 413, 282-285 (2001) and cond-mat/0107347.
- [6] T. Hanaguri, C. Lupien, Y. Kohsaka, D. -H. Lee, M. Azuma, M. Takano, H. Takagi, J. C. Davis, Nature 430, 1001 (2004).
- [7] Patrick A. Lee, Naoto Nagaosa, Xiao-Gang Wen, Rev. Mod. Phys. **78**, 17 (2006).
- [8] J. Bobroff, H. Alloul, S. Ouazi, P. Mendels, A. Mahajan, N. Blanchard, G. Collin, V. Guillen, and J.-F. Marucco, Phys. Rev. Lett.**89** 157002 (2002).
- [9] J.W. Loram, J.L. Tallon, and W. Y. Liang, Phys. Rev. **B69**, 060502 (2004).
- [10] E.V.L. de Mello, and E.S. Caixeiro, Phys. Rev. **.B70**, 224517 (2004).
- [11] A. Damascelli, Z. Hussain, and Z.-X. Shen, Rev. Mod. Phys. **75**, 473 (2003)
- [12] X. J. Zhou, T. Yoshida, S. A. Kellar1, P. V. Bogdanov, E. D. Lu, A. Lanzara, M. Nakamura, T. Noda, T. Kakeshita, H. Eisaki, S. Uchida, A. Fujimori, Z. Hussain, and Z.-X. Shen, Phys. Rev. Lett.**86**, 5578 (2001),
- [13] X. J. Zhou, T. Yoshida, D.-H. Lee, W. L. Yang, V. Brouet, F. Zhou, W. X. Ti, J. W. Xiong, Z. X. Zhao, T. Sasagawa, T. Kakeshita, H. Eisaki, S. Uchida, A. Fujimori Z. Hussain and Z.-X. Shen, Phys. Rev. Lett.**92**, 187001 (2004).
- [14] A. Ino, I. C. Kim, M. Nakamura, T. Yoshida, T. Mizokawa, A. Fujimori, Z.-X. Shen, T. Kakeshita, H. Eisaki, and S. Uchida, Phys. Rev. **B65**, 094504.
- [15] C. Howald, P. Fournier, and A. Kapitulnik, Phys. Rev. **B64**, 100504 (2001).
- [16] K.M. Lang, V. Madhavan, J.E. Hoffman, E.W. Hudson, H. Eisaki, S. Uchida and J.C. Davis, Nature, **415**, 412 (2002).
- [17] J. E. Hoffman, K. McElroy, D.-H. Lee, K. M Lang, H. Eisaki, S. Uchida, J.C. Davis, Science **297**, 1148-1151 (2002).
- [18] K. McElroy, R.W Simmonds, J. E. Hoffman, D.-H. Lee, J. Orenstein, H. Eisaki, S. Uchida, J.C. Davis, Nature, **422**, 520 (2003).
- [19] A. C. Fang, L. Capriotti, D. J. Scalapino, S. A. Kivelson, N. Kaneko, M. Greven, and A. Kapitulnik, Phys. Rev. Lett.**96**, 017007 (2006).
- [20] K. McElroy, D.-H. Lee, J. E. Hoffman, K.M. Lang, J. lee, E. W. Hudson, H. Eisaki, S. Uchida, J.C. Davis, Phys. Rev. Lett., **94**, 197005 (2005).
- [21] Michael Vershinin, Shashank Misra, S. Ono, Y. Abe, Yoichi Ando, Ali Yazdani, Science **303**, 1995 (2004).
- [22] Ch. Renner, B. Revaz, J.Y. Genoud, K. Kadowaki, O. Fischer, Phys. Rev. Lett.**80**, 149 (1998).
- [23] N. Miyakawa, P. Guptasarma, J. F. Zasadzinski, D. G. Hinks, and K. E. Gray , Phys. Rev. Lett.**80**, 157 (1998).
- [24] Minoru Suzuki, and Takao Watanabe, Phys. Rev. Lett.**85** 4787, (2000).
- [25] Guy Deutscher, Nature **397**, 410 (1999).
- [26] V.M. Krasnov, A. E. Kovalev, A. Yurgens, and D. Winkler Phys. Rev. Lett. **86** 2657 (2001).
- [27] A. Yurgens, D. Winkler, T. Claeson, S. Ono, and Yoichi Ando, Phys. Rev. Lett. **90**, 147005 (2003).
- [28] A. Mourachkine, Physica **341-348**, 917 (2000).
- [29] A. Mourachkine, Review article in Modern Physics Let-



- ters **B19**, 743 (2005), and cond-mat/0506732.
- [30] A. Bianconi, N.L. Saini, A. Lanzara, M. Missori, T. Rossetti, H. Oyanagi, H. Yamaguchi, K. Oda and T. Ito, Phys. Rev. Lett. **76**, 3412 (1996).
- [31] E.S. Bozin, G.H. Kwei, H. Takagi, and S.J.L. Billinge, Phys. Rev. Lett. **84**, 5856, (2000).
- [32] N. J. Curro, P. C. Hammel, B. J. Suh, M. Hcker, B. Bchner, U. Ammerahl, and A. Revcolevschi, Phys. Rev. Lett. **85**, 642 (2000).
- [33] P. M. Singer, A. W. Hunt, and T. Imai, Phys. Rev. Lett. **88**, 047602 (2002).
- [34] J. Haase, O. P. Sushkov, P. Horsch, and G. V. M. Williams, Phys. Rev. **B69**, 094504 (2004).
- [35] H. J. Grafe, N. J. Curro, M. Hcker, and B. Behner, Phys. Rev. Lett. **96**, 017002 (2006).
- [36] J. Zaanen, and O. Gunnarson, Phys. Rev. **B40**, 7391 (1989).
- [37] M. Kato, K. Machida, H. Nakanishi, and M. Fujita, J. Phys. Soc. Jpn., **59**, 1047 (1990).
- [38] J.C. Grenier, N. Lagueyte, A. Wattiaux, J.P. Doumerc, P. Dordor, J. Etourneau, M. Puchard, J. B. Goodenough, and J.S. Zhou, Phys. **C202**, 209 (1992).
- [39] J. D. Jorgensen, B. Dabrowski, Shiyu Pei, D. G. Hinks, L. Soderholm, B. Morosin, J. E. Schirber, E. L. Venturini, and D. S. Ginley Phys. Rev. **B38**, 11337 (1988).
- [40] M. Truccato, C. Lamberti, C. Prestipino, A. Agostino, Appl. Phys. Lett. **86**, 213116, (2005), and cond-mat/506198.
- [41] N. Kristoffel, and P. Rubin, Physica **C418**, 49 (2005).
- [42] R. S. Markiewicz, Phys. Rev. Lett. **89**, 229703 (2002).
- [43] J.W. Cahn and J.E. Hilliard, J. Chem. Phys, **28**, 258 (1958).
- [44] E.V.L de Mello, and Otton T. Silveira Filho Physica **A347**, 429 (2005).
- [45] Yu.N. Ovchinnikov, S.A. Wolf, and V.Z. Kresin, Phys. Rev. **B63**, 064524, (2001), and Physica **C341-348**, 103, (2000).
- [46] E.V.L. de Mello, E.S. Caixeiro, and J.L. González, Phys. Rev. **B67**, 024502 (2003).
- [47] J.L. González, and E.V.L. de Mello, Phys. Rev. **B 69**, 134510 (2004).
- [48] S. H. Naqib, J. R. Cooper, J. L. Tallon, R. S. Islam, and R. A. Chakalov, Phys. Rev. **B71**, 054502 (2005).
- [49] M. Franz, C. Kallin, A.J. Berlinsky, and M.I. Salkola, Phys. Rev. B **56**, 7882 (1997).
- [50] A. Ghosal, M. Randeria, and N. Trivedi, Phys. Rev. **B63**, R020505 (2000).
- [51] A. Ghosal, M. Randeria, and N. Trivedi, Phys. Rev. B **65**, 014501 (2001).
- [52] Tamara S. Nunner, Brian M. Andersen, Ashot Melikyan, and P. J. Hirshfeld, Phys. Rev. Lett. **95**, 177003 (2005).
- [53] M. C. Schabel, C. -H. Park, A. Matsuura, Z.-X. Shen, D.A. Bonn, X. Liang, W.N. Hardy, Phys. Rev. B **57**,6090 (1998).
- [54] "Introduction to Percolation Theory", D. Stauffer, and A. Aharony, Taylor & Francis Ed., 2nd. Edition, Bristol, (1994).
- [55] N. Bergeal, J. Leuseur, M. Aprili, F. Faini, J. P. Contour and B. Leridon, cond-mat/0601265.
- [56] V.J. Emery, and S.A. Kivelson, Nature, **374**, 434 (1995).
- [57] T. Yoshida, X. J. Zhou, T. Sasagawa, W. L. Yang, P. V. Bogdanov, A. Lanzara, Z. Hussain, T. Mizokawa, A. Fujimori, H. Eisaki, Z.-X. Shen, T. Kakeshita, and S. Uchida Phys. Rev. Lett. **91**, 027001, (2003).
- [58] Yayu Wang, Lu Li, and N. P. Ong, Phys. Rev. **B73**, 024510, (2006).